2009 American Control Conference
Hyatt Regency Riverfront, St. Louis, MO, USA
June 10-12, 2009

Optimal Performance Trade-offs in Repetitive Control: Experimental Validation on an Active Air Bearing Setup

Goele Pipeleers, Bram Demeulenaere, Farid Al-Bender, Joris De Schutter, Jan Swevers
Katholieke Unviversiteit Leuven, Dept. of Mechanical Engineering
Celestijnenlaan 300B, B-3001 Heverlee, Belgium
goele.pipeleers@mech.kuleuven.be

Abstract— **In repetitive control, the Bode Sensitivity Integral dictates a fundamental trade-off between improved suppression of periodic disturbances and degraded performance for non-periodic inputs. This paper experimentally demonstrates the implications of this trade-off by applying a recently developed systematic repetitive control design approach to an active air bearing setup. This design methodology translates the fundamental trade-off into trade-off curves between a non-periodic and periodic performance index, of which the practical relevance is illustrated by the obtained experimental results.**

I. Introduction

Including a repetitive controller in the feedback loop constitutes a common way to improve the attenuation of periodic disturbances. However, this improved periodic performance comes at the price of degraded performance for non-periodic inputs, since pushing the sensitivity down to zero at the periodic input's harmonics increases the sensitivity at intermediate frequencies, as dictated by the Bode Sensitivity Integral [4]. To allow for a systematic analysis of this fundamental trade-off in repetitive control, Pipeleers et al. [12] define two performance indices quantifying the repetitive controller's effect on the closed-loop performance with respect to periodic and non-periodic inputs. Period-time uncertainty is explicitly accounted for and the repetitive controller is designed to yield an optimal trade-off between both performance indices. By application of the (generalized) Kalman-Yakubovich-Popov (KYP) lemma [9], the corresponding optimal design problem is translated into a semi-definite program (SDP), of which the convexity (i) guarantees the reliable and efficient computation of the global optimum, and (ii) facilitates the generation of trade-off curves between the two conflicting performance indices.

The purpose of this paper is to experimentally demonstrate the value of the trade-off curves computed by the approach [12] in dealing with the fundamental performance trade-off in repetitive control on an active air bearing setup. The control objective is reducing the error motion of the spindle's axis of rotation by appropriate actuation of the active journal bearing. This error motion, being related to mass unbalance and profile errors of the bearing parts, is periodic with the spindle rotation, leaving measurement noise as the sole non-periodic input to the control problem. Comparison of various repetitive controller designs on the trade-off curve reveal that superior reduction of the periodic error motion comes at too high a price of measurement noise amplification. This deteriorates the overall closed-loop performance while the trade-off curve reveals more appropriate repetitive controller designs.

As periodic disturbances are characteristic for spindle applications, repetitive control is not new in the field of active bearing control. In active air bearing applications, repetitive control has been applied to overcome the low stiffness and damping of the air film [2], [6], [7], whereas in magnetic bearings, repetitive control is essential for obtaining sufficient rotational accuracy [16], [17]. While in these applications the repetitive controller is restricted to a basic, first-order design, more advanced repetitive controller designs have been experimentally validated for disk drive servo systems [14], [15], a major industrial application of repetitive control. However, all these repetitive controllers enforce perfect suppression of the periodic disturbances without investigating the consequences of the fundamental trade-off in repetitive control on the overall performance.

This paper is organized as follows. Section II first describes the experimental setup and the corresponding control scheme. Section III elaborates on the repetitive controller design, while Sec. IV experimentally validates the selected controllers. Section V concludes the paper. The notation used in this paper is standard. To alleviate notation, the frequency response function (FRF) of a discrete-time system $H(z)$ is denoted by $H(\omega)$ instead of $H\left(e^{j\omega T_s}\right)$.

II. Experimental Setup

The experimental setup comprises the active air bearing prototype presented in [1]. Section II-A starts with the description of the test setup, whereas Sec. II-B details the corresponding control scheme. Subsequently, Sec. II-C discusses the parametric identification of the system.

A. Description

The experimental setup is depicted in Fig. 1, where Fig. 1(a) shows a top view of the setup and Fig. 1(b) illustrates the active air bearing layout.

The spindle is driven by an asynchronous motor and supported by aerostatic bearings: the axial (thrust) and rear radial (journal) bearing are passive whereas the front radial bearing is active. The active bearing comprises a compliant bearing surface composed of four lands, which are supported

978-1-4244-4524-0/09/$25.00 ©2009 AACC

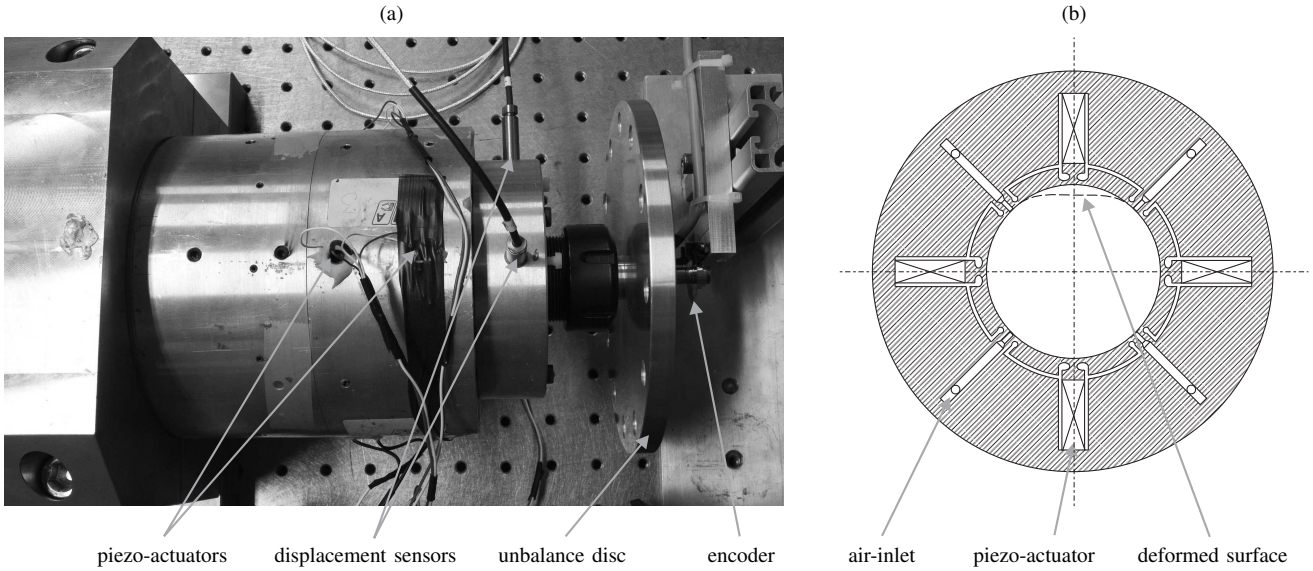

Fig. 1. Active air bearing setup: (a) top view of the experimental setup and (b) illustration of the active air bearing layout (not proportional), where the dashed line illustrates the bearing surface deformation due to actuation of the top piezo-actuator.

on four rows of two piezo-actuators each. These actuators deform the bearing surface in a controlled manner so as to induce a radial force on the shaft via the air film. In the case of the radial spindle bearing, the shaft has two degrees of freedom normal to its axis. Consequently, two displacement sensors are needed, one for each of these two principal directions. Capacitive sensors are employed (Lion Precision) and a reference target ring was machined in situ on the spindle nose. The two measurement directions are aligned horizontally and vertically, and coincide with the working directions of the piezo-actuators. When driving the opposite piezo-actuators in anti-phase, both "pushing" and "pulling" in the two principal directions is possible. As a result, only two scalar control inputs, denoted u_h [V] and u_v [V], remain determining the amplifier inputs for the horizontal and vertical piezo-actuators, respectively. These signals are grouped into the vector

$$\mathbf{u} = \begin{bmatrix} u_h \\ u_v \end{bmatrix} , \tag{1}$$

and in the same way, the outputs of the displacement sensors, denoted $y_{m,h}$ [m] and $y_{m,v}$ [m], are grouped into $\mathbf{y_m}$. Throughout this paper, vectors and matrices are indicated in bold, where in case of a two-dimensional vector, the first and second element relate to the horizontal and vertical direction, respectively.

At the nose of the spindle, a disk is clamped generating a $4.6\,10^{-5}$ kgm mass unbalance and at the end of this disk an encoder (500 counts per rotation) is mounted.

B. Control scheme

The objective of the controller is to suppress the error motion $\mathbf{e}$ [m] of the spindle's axis of rotation by controlling the piezo-actuators of the active air bearing based on the measured displacements $\mathbf{y_m}$ [m]. Since $\mathbf{e}$ is periodic with the spindle rotation, repetitive control is the appropriate control strategy. The control problem is handled in discrete time, where the sample frequency equals $f_s = 10$ kHz and the corresponding control scheme is shown in Fig. 2. The experimental validation of the repetitive controllers focusses on rotational speeds of the spindle between 900 rpm and 1200 rpm.

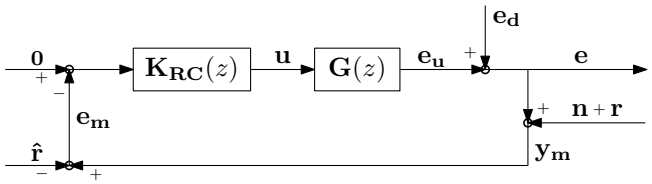

Fig. 2. Control scheme used to suppress the error motion of the spindle's axis of rotation by repetitive control.

The error motion $\mathbf{e}$ is the sum of two contributions: (i) $\mathbf{e_d}$ [m] related to the mass unbalance and profile errors of the bearing parts and (ii) $\mathbf{e_u}$ [m] caused by actuation of the active air bearing. The displacement sensors generate the measurement $\mathbf{y_m}$, which corresponds to the actual error motion $\mathbf{e}$ corrupted with (i) (stochastic) measurement noise $\mathbf{n}$ [m] and (ii) a (periodic) systematic error $\mathbf{r}$ [m] due to roundness error of the reference target ring for the displacement sensors.

As suppressing the error motion $\mathbf{e}$ constitutes the control objective, the repetitive controller $\mathbf{K_{RC}}(z)$ should not respond to the systematic measurement error $\mathbf{r}$. To this end, the measured error motion $\mathbf{e_m}$ [m] is constructed from the measurements $\mathbf{y_m}$ by subtracting an estimate $\hat{\mathbf{r}}$ [m] of the roundness error $\mathbf{r}$. To compute $\hat{\mathbf{r}}$ at each time instant, the roundness error is determined a priori as a function of the spindle angle θ [rad] using the method of master reversal proposed by Donaldson [3]. In operation θ is measured by the encoder, yielding $\hat{\mathbf{r}}$ as a function of time.

C. Identification

For the considered control problem, the plant $\mathbf{G}(z)$ corresponds to the two-by-two system with input $\mathbf{u}$ and output

$\mathbf{e_u}$:

$$\underbrace{\begin{bmatrix} e_{u,h} \\ e_{u,v} \end{bmatrix}}_{\mathbf{e_u}} = \underbrace{\begin{bmatrix} G_h(z) & G_{hv}(z) \\ G_{vh}(z) & G_v(z) \end{bmatrix}}_{\mathbf{G}(z)} \underbrace{\begin{bmatrix} u_h \\ u_v \end{bmatrix}}_{\mathbf{u}} . \tag{2}$$

The identification is performed by separate excitation of the horizontal and vertical piezo-actuators and is executed at three rotational speeds of the spindle: 900 rpm, 1050 rpm and 1200 rpm. The system is excited between 1 Hz and 2500 Hz by random multi-sines [11] with a frequency resolution of 1 Hz. The error motion $\mathbf{e_d}$ (due to mass unbalance and profile errors of the bearing parts) does not hamper the identification, for the excitation frequencies are selected not to coincide with harmonics of the spindle's rotational speed.

The non-parametric FRF estimates for the four plant components reveal that (i) the off-diagonal gains $|G_{hv}(\omega)|$ and $|G_{vh}(\omega)|$ are on average 20 dB less than the diagonal gains $|G_h(\omega)|$ and $|G_v(\omega)|$, and (ii) up to 1 kHz, the plant dynamics are almost independent of the spindle's rotational speed. Based on the first observation, the plant is assumed decoupled for the controller design and the simulations, that is: the off-diagonal components $G_{hv}(z)$ and $G_{vh}(z)$ are neglected. The subsequent experimental validation of the controllers supports this assumption, for the experimental results on the actual, coupled setup show good correspondence with the decoupled simulations.

Given the decoupling assumption, the controller design only requires parametric models for the diagonal plant components $G_h(z)$ and $G_v(z)$. Using the fdident toolbox [10], a 9th order discrete-time model $\widehat{G}_h(z)$ is identified for $G_h(z)$, while the identified model $\widehat{G}_v(z)$ for $G_v(z)$ is of order 17. Comparison of the parametric and non-parametric FRFs indicate that both plant models are accurate up to 600 Hz.

III. Repetitive Controller Design

This section elaborates on the design of the repetitive controller $\mathbf{K_{RC}}(z)$. Relying on the decoupling assumption for the plant $\mathbf{G}(z)$, a decoupled design of the repetitive controller $\mathbf{K_{RC}}(z)$ suffices:

$$\mathbf{K_{RC}}(z) = \begin{bmatrix} K_{RC,h}(z) & 0 \\ 0 & K_{RC,v}(z) \end{bmatrix} , \tag{3}$$

where the SISO controllers $K_{RC,h}(z)$ and $K_{RC,v}(z)$ are designed according to the strategy proposed in [12]. Section III-A summarizes this design approach, while Sec. III-B discusses the selected repetitive controllers for the control problem at hand.

Concerning the rotational speed of the spindle, the following notation is used: The desired rotational speed used as entry for the frequency converter that drives the asynchronous motor is indicated by $f_{0,\text{des}}$ [Hz]. However, the repetitive controller implementation requires the period to contain an integer number N of samples. Hence, assuming that f_s cannot be changed, the best the repetitive controller can do is to account for $f_0 = f_s/N$ [Hz], where

$$N = \text{int}(f_s/f_{0,\text{des}}) , \tag{4}$$

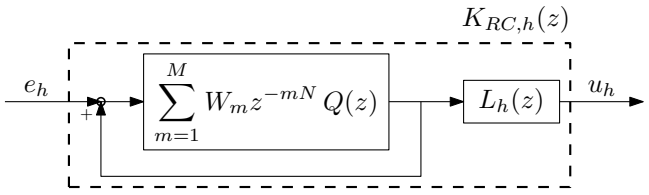

Fig. 3. Structure of the horizontal SISO repetitive controller, where the vertical equivalent is obtained by replacing the subscript $\cdot_h$ by $\cdot_v$.

and $\omega_0 = 2\pi f_0$ [rad/s]. The actual rotational speed of the spindle is denoted $f_{0,\delta}$ [Hz] ($\omega_{0,\delta} = 2\pi f_{0,\delta}$ [rad/s]) and may deviate from both $f_{0,\text{des}}$ and f_0, where δ corresponds to the relative deviation from f_0

$$f_{0,\delta} = f_0(1+\delta) , \tag{5}$$

and is bounded by Δ:

$$|\delta| < \Delta . \tag{6}$$

A. Repetitive controller design strategy

The SISO repetitive controllers $K_{RC,h}(z)$ and $K_{RC,v}(z)$ feature the structure of Fig. 3, where only the design of the filter $L(z)$ depends on the control direction. The horizontal repetitive controller equals

$$K_{RC,h}(z) = L_h(z)\,\frac{W(z)Q(z)}{1-W(z)Q(z)} , \tag{7}$$

where

$$W(z) = \sum_{m=1}^{M} W_m z^{-mN} , \tag{8}$$

and N is given by (4). M is called the order of the repetitive controller. Under the assumption of a decoupled plant, the decoupled controller $\mathbf{K_{RC}}(z)$ (3) gives rise to a decoupled closed-loop sensitivity function, of which the horizontal diagonal element is given by

$$S_h(z) = \frac{1-W(z)Q(z)}{1-W(z)Q(z)\,[1-L_h(z)G_h(z)]} . \tag{9}$$

The vertical equivalents of (7) and (9) are obtained by replacing the subscript $\cdot_h$ by $\cdot_v$.

The filters $Q(z)$ and $L(z)$ guarantee robust stability of the closed-loop system, whereas the closed-loop performance is optimized through the design of $W(z)$.

1) Stability: To achieve robust closed-loop stability, the filters $L(z)$ and $Q(z)$ are designed in accordance with the common procedure in repetitive control [5], [8], [14]:

- $L(z)$ is designed as the series connection of the inverse plant model and a low-pass filter $F(z)$:

$$L_h(z) = \widehat{G}_h(z)^{-1}F(z) , \quad L_v(z) = \widehat{G}_v(z)^{-1}F(z) , \tag{10}$$

where the relative degree of the minimum-phase but strictly proper identified plant models is accounted for as explained in [15]. $F(z)$ is designed as a low-pass linear-phase FIR filter[1] of order 300 with cut-off frequency 640 Hz.

[1]Linear-phase FIR filters are preferred for $F(z)$ and $Q(z)$, since their linear phase behavior can be compensated for, as detailed in [15].

- $Q(z)$ is designed as a low-pass linear-phase FIR filter of order 200 with cut-off frequency 620 Hz.

Including the inverse plant model in $L(z)$ guarantees nominal stability, for in case of perfect plant models $\widehat{G}_h(z)$ and $\widehat{G}_v(z)$ and $F(z) = Q(z) = 1$, $S_h(z)$ and $S_v(z)$ are both equal to:

$$\widetilde{S}(z) = 1 - W(z) \; . \tag{11}$$

However, the identified models are only accurate up to 600 Hz, raising the issue of robust stability. To this end, the low-pass filters $Q(z)$ and $F(z)$ turn off the repetitive controller from 600 Hz, the frequency from which the identified models are insufficiently accurate.

2) Performance: According to [12], performance is specified as an optimal trade-off between two performance indices that quantify the closed-loop performance with respect to the periodic and the non-periodic inputs, respectively. The definition of these performance indices relies on the assumptions that in the pass band of the filters $Q(z)$ and $F(z)$ (i) the filters equal their dc-gain and (ii) the identified plant models are perfect. These assumptions imply that $S_h(\omega) = S_v(\omega) = \widetilde{S}(\omega)$ holds up to 600 Hz.

The *periodic performance index* $\gamma_{p,\Delta}$ corresponds to the smallest reduction $|\widetilde{S}(l\omega_{0,\delta})|$ over all harmonics $l \leq \Lambda$ and over all potential $\omega_{0,\delta}$ values:

$$\gamma_{p,\Delta} \equiv \max_{l \leq \Lambda} \left\{ \max_{\omega \in \Omega_l} \left\{ |\widetilde{S}(\omega)| \right\} \right\} \; , \tag{12}$$

where Ω_l corresponds to the uncertainty interval on the lth harmonic:

$$\Omega_l = [l\omega_0(1-\Delta) \; , \; l\omega_0(1+\Delta)] \; . \tag{13}$$

Λ is set equal to the highest harmonic in the pass-band of $Q(z)$ that should be suppressed. Attenuation of the periodic disturbances corresponds to $\gamma_{p,\Delta} < 1$, where $\gamma_{p,\Delta} = 0$ indicates perfect rejection.

The *non-periodic performance index* γ_{np} is defined as the highest amplification $|\widetilde{S}(\omega)|$ over all frequencies ω:

$$\gamma_{np} \equiv \|\widetilde{S}(\omega)\|_\infty \; . \tag{14}$$

Due to the Bode Sensitivity Integral, repetitive controllers are bound to amplify the non-periodic disturbances, yielding $\gamma_{np} > 1$, where values closer to one are preferred.

The repetitive controller is designed to yield an optimal trade-off between the conflicting performance indices $\gamma_{p,\Delta}$ and γ_{np}. To this end, the parameters W_m are computed as the solution of the following optimization problem

$$\begin{aligned} \underset{W_m}{\text{minimize}} \quad & \gamma_{p,\Delta} + \alpha\gamma_{np} && \text{(15a)} \\ \text{subject to} \quad & \text{def. (12)} && \text{(15b)} \\ & \text{def. (14)} \; , && \text{(15c)} \end{aligned}$$

where the weight α quantifies the relative importance of $\gamma_{p,\Delta}$ and γ_{np}. As explained in [12], application of the (generalized) KYP lemma converts this optimization problem into an SDP. The convexity of the obtained optimization problem guarantees the reliable and efficient computation of the global optimum and facilitates the generation of trade-off curves between $\gamma_{p,\Delta}$ and γ_{np}, which are computed by solving (15) for a range of α values.

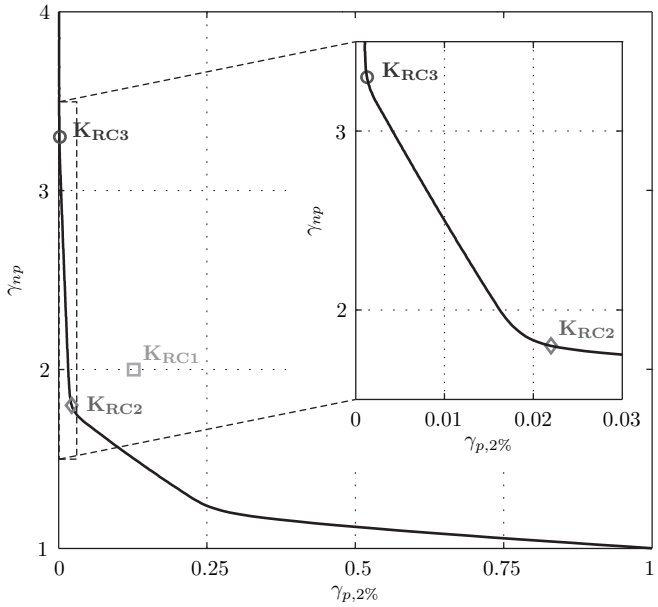

Fig. 4. Trade-off curve between $\gamma_{p,2\%}$ and γ_{np} for fifth-order repetitive controllers, where the selected controller designs are indicated. $\mathbf{K_{RC2}}(z)$ and $\mathbf{K_{RC3}}(z)$ correspond to optimal fifth-order repetitive controllers, whereas $\mathbf{K_{RC1}}(z)$ is a classical first-order controller.

B. Selected repetitive controllers

As explained in [12], given $W(z)$, $\gamma_{p,\Delta}$ depends only on the product $\Lambda\Delta$ and neither on f_0, nor on the individual values of Λ and Δ. In the repetitive controller design $\Lambda\Delta$ is set equal to 2% and with an abuse of notation the periodic performance index is indicated by $\gamma_{p,2\%}$ instead of $\gamma_{p,\Delta}$.

Three repetitive controllers, characterized by a different design of $W(z)$ and of which the corresponding performance indices are given in Table I, are experimentally validated. The first repetitive controller, denoted $\mathbf{K_{RC1}}(z)$, corresponds to the more frequently used basic first-order repetitive controller $W(z) = z^{-N}$. This controller yields $\gamma_{np} = 2$ and although this controller perfectly rejects periodic disturbances at f_0, its robust periodic performance is moderate: $\gamma_{p,2\%} = 0.13$.

The repetitive controllers $\mathbf{K_{RC2}}(z)$ and $\mathbf{K_{RC3}}(z)$, on the other hand, are fifth-order repetitive controllers ($M = 5$), optimized according to (15) and corresponding to different trade-offs between $\gamma_{p,2\%}$ and γ_{np} (that is: different weights α). Figure 4 indicates both designs on the trade-off curve between $\gamma_{p,2\%}$ and γ_{np} for fifth-order repetitive controllers. For a given level of robust periodic performance $\gamma_{p,2\%}$, the trade-off curve indicates the minimal level of non-periodic performance degradation γ_{np} that has to be tolerated. Or, vice-versa, for a fixed level of non-periodic performance, the trade-off curve indicates the best robust periodic performance that can be achieved. The steep slope between $\mathbf{K_{RC2}}(z)$ and $\mathbf{K_{RC3}}(z)$ indicates that improving the periodic performance below $\gamma_{p,2\%} = 0.022$ comes at the price of very high amplification of the non-periodic disturbances: compared

	$\gamma_{p,2\%}$	γ_{np}
$\mathbf{K_{RC1}}(z)$	0.13	2
$\mathbf{K_{RC2}}(z)$	0.022	1.8
$\mathbf{K_{RC3}}(z)$	0.0013	3.3

TABLE I

PERFORMANCE INDICES OF THE SELECTED REPETITIVE CONTROLLERS.

to $\mathbf{K_{RC2}}(z)$, $\mathbf{K_{RC3}}(z)$ improves the periodic performance from $\gamma_{p,2\%} = 0.022$ to $\gamma_{p,2\%} = 0.0013$, but degrades the non-periodic performance from $\gamma_{np} = 1.8$ to $\gamma_{np} = 3.3$. The first-order repetitive controller $\mathbf{K_{RC1}}(z)$ is also indicated in Fig. 4, but as it does not correspond to an optimal fifth-order design, it is located off the trade-off curve.

IV. EXPERIMENTAL RESULTS

This section investigates the implications of the fundamental performance trade-off in repetitive control on the active air bearing setup by comparing the selected repetitive controllers. The experimental validation is performed at various spindle speeds between 900 rpm and 1200 rpm, but as these results are very similar, this section only discusses the validation at 1200 rpm, yielding $f_0 = f_{0,\text{des}} = 20$ Hz and $N = 500$.

To distinguish between the conflicting performance aspects of the repetitive controllers, the measured steady-state error motion $\mathbf{e_m}$ is split up in its part periodic with the spindle rotation and its non-periodic contribution. Table II summarizes the root-mean-square (rms) values of the periodic and non-periodic part of $\mathbf{e_m}$, where only the frequency content up to 600 Hz, the working range of the repetitive controllers, is accounted for. This table is further discussed below.

A. Periodic performance

To allow for a detailed evaluation of the repetitive controllers's periodic performance, Fig. 5 shows the reduction in the amplitude spectrum of the periodic part of the measured horizontal error motion $e_{m,h}$ achieved by the repetitive controllers. The actual period of the spindle rotation is estimated using the approach of [13], yielding $f_{0,\delta} = 19.968$ Hz, and the spectrum is shown up to the 30th harmonic.

Converted to dB, the $\gamma_{p,2\%}$-values of Table I imply that all harmonics up to $\Lambda = \text{int}(2\%/\Delta)$ will be reduced by 18 dB by $\mathbf{K_{RC1}}(z)$, 33 dB by $\mathbf{K_{RC2}}(z)$, and 58 dB by $\mathbf{K_{RC3}}(z)$. As $f_{0,\delta} = 19.968$ Hz corresponds to $\delta = 0.16\%$, it follows that this theoretical result should be valid for $\Lambda = 12$, as confirmed by Fig. 5. Furthermore, both Fig. 5 and Table II indicate that a lower $\gamma_{p,2\%}$ value gives rise to a smaller periodic contribution to $\mathbf{e_m}$, even if 30 harmonics are taken into account.

The results for $\mathbf{K_{RC1}}(z)$ reveal the necessity to account for uncertainty on f_0. Whereas this controller would perfectly eliminate the periodic contribution to $\mathbf{e_m}$ if $\delta = 0\%$, the small deviation $\delta = 0.16\%$ causes a significant periodic performance degradation for $\mathbf{K_{RC1}}(z)$.

	horizontal		vertical	
	per.	non-per.	per.	non-per.
no RC	95.2 nm	2.4 nm	113.4 nm	2.9 nm
$\mathbf{K_{RC1}}(z)$	4.3 nm	2.1 nm	3.9 nm	3.9 nm
$\mathbf{K_{RC2}}(z)$	2.7 nm	2.1 nm	2.7 nm	4.2 nm
$\mathbf{K_{RC3}}(z)$	0.7 nm	4.4 nm	0.9 nm	8.6 nm

TABLE II

STEADY-STATE RESPONSE (1200 RPM): ROOT-MEAN-SQUARE VALUES OF THE PERIODIC AND NON-PERIODIC CONTRIBUTION TO THE MEASURED ERROR OF THE SPINDLE'S AXIS OF ROTATION IN THE ACTIVE FREQUENCY RANGE OF THE REPETITIVE CONTROLLERS.

B. Non-periodic performance

For the control problem at hand, the measurement noise $\mathbf{n}$ constitutes the sole non-periodic input to the closed-loop system. Figure 6 complements the rms values of Table II by showing the power spectrum of the non-periodic part of the measured error motion $\mathbf{e_m}$.

Converted to dB, the γ_{np}-values of Table I translate into a worst-case measurement noise amplification of 6 dB by $\mathbf{K_{RC1}}(z)$, 5 dB by $\mathbf{K_{RC2}}(z)$ and 10 dB by $\mathbf{K_{RC3}}(z)$. As observed in Fig. 6, these amplification levels manifest in between the harmonics. Inspection of the rms values in Table II reveals that the superior periodic performance of $\mathbf{K_{RC3}}(z)$ comes at too high an amplification of the measurement noise, deteriorating the overall closed-loop performance. From this point of view $\mathbf{K_{RC2}}(z)$ is preferred, for it combines better periodic performance than $\mathbf{K_{RC1}}(z)$ with a similar amplification of measurement noise.

Interpretation of the results of Fig. 6 and Table II requires special care, for they involve the *measured* error motion $\mathbf{e_m}$. While $\mathbf{n}$ relates to $\mathbf{e_m}$ by the closed-loop sensitivity, its effect on the *actual* error motion $\mathbf{e}$ is determined by the complementary sensitivity. However, simulation of the measured actuator signals through the identified plant models $\widehat{G}_h(z)$ and $\widehat{G}_v(z)$ (providing an estimate of the actuals error motion $\mathbf{e}$) yields similar results as Fig. 6 and Table II, and hence, the main conclusions regarding the non-periodic performance remain valid.

V. CONCLUSION

Relying on the repetitive controller design methodology of [12], this paper investigates the implications of the fundamental performance trade-off in repetitive control for the reduction of the error motion of the spindle's axis of rotation in an active air bearing setup. As dictated by the Bode Sensitivity Integral, improved suppression of periodic disturbances, quantified by $\gamma_{p,\Delta}$, comes at the price of degraded performance for non-periodic inputs, quantified by γ_{np}.

The experimental results confirm the trade-off curve between $\gamma_{p,\Delta}$ and γ_{np}, as computed by [12]. Although measurement noise constitutes the sole non-periodic input to the considered control problem, the experimental results show that it should not be neglected in the repetitive controller design. If $\gamma_{p,\Delta}$ is improved at the price of too high a degra-

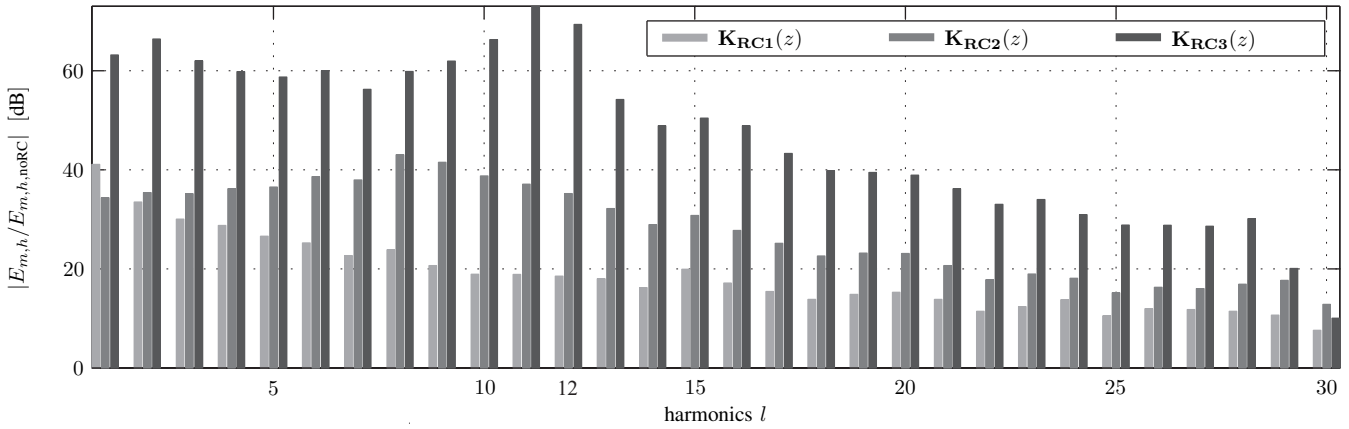

Fig. 5. Periodic steady-state response (1200 rpm): reduction in the amplitude spectrum of the periodic part of the horizontal tracking error $e_{m,h}$ achieved by the three repetitive controllers.

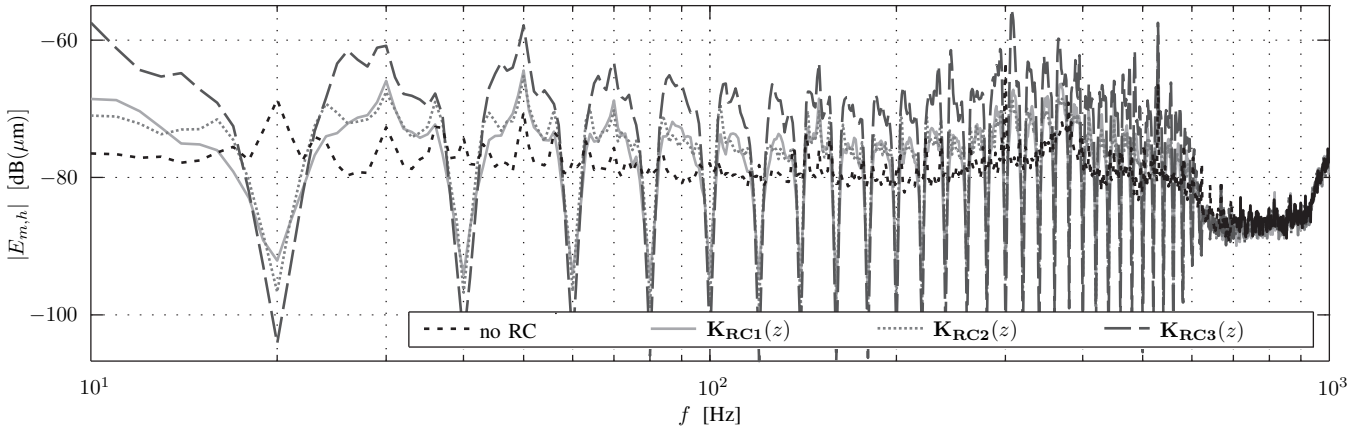

Fig. 6. Non-periodic steady-state response (1200 rpm): power spectrum of the non-periodic component of the measured horizontal error motion $e_{m,h}$ for the three repetitive controllers.

dation of γ_{np}, the fed-back measurement noise dominates the error motion of the axis of rotation.

ACKNOWLEDGMENT

Goele Pipeleers is a Research Assistant of the Research Foundation - Flanders (FWO–Vlaanderen) and Bram Demeulenaere is a Postdoctoral Fellow of the Research Foundation - Flanders. This work benefits from K.U.Leuven-BOF EF/05/006 Center-of-Excellence Optimization in Engineering and from the Belgian Programme on Interuniversity Attraction Poles, initiated by the Belgian Federal Science Policy Office.

REFERENCES

[1] F. Al-Bender and H. Van Brussel. Development of high frequency electrospindles with passive and active air bearings. In *Proceedings of the International Seminar on Improving Machine Tool Performance*, pages 175–184, San Sebastian, Spain, July 1998.

[2] F. Al-Bender, H. Van Brussel, and P. Vanherck. Actively compensated aerostatic bearings. In *Proceedings of the ASPE 2001, Precision Bearings and Spindles, Summer Tropical Meeting*, June 2001.

[3] R. R. Donaldson. A simple method for separating spindle error from test ball roundness error. *Annals of the CIRP*, 21(1):125–126, 1972.

[4] J. S. Freudenberg and D. P. Looze. Right half plane poles and zeros and design trade-offs in feedback systems. *IEEE Transactions on Automatic Control*, AC-30(6):555–565, 1985.

[5] S. Hara, Y. Yamamoto, T. Omata, and M. Nakano. Repetitive control system: A new type of servo system for periodic exogenous signals. *IEEE Transactions on Automatic Control*, 33(7):695–668, 1988.

[6] O. Horikawa, K. Sato, and A. Shimokohbe. An active air journal bearing. *Nanotechnology*, 3:84–90, 1992.

[7] O. Horikawa and A. Shimokohbe. An active air bearing. *JSME International Journal, Series 3*, 33(1):55–60, 1990.

[8] T. Inoue. Practical repetitive control system design. In *Proc. of the 29th IEEE Conference on Decision and Control*, pages 1673–1678, Honolulu, Hawaii, December 1990.

[9] T. Iwasaki and S. Hara. Generalized kyp lemma: unified frequency domain inequalities with design applications. *IEEE Transactions on Automatic Control*, 50(1):41–59, 2005.

[10] I. Kollar. Frequency domain system identificaton toolbox v3.3 for matlab", gamax ltd, budapest. 2004-2007.

[11] R. Pintelon and J. Schoukens. *Systems Identification: A Frequency Domain Approach*. Institute of Electrical and Electronics Engineers, Inc., New York, USA, 2001.

[12] G. Pipeleers, B. Demeulenaere, J. Swevers, and J. De Schutter. Robust high-order repetitive control: optimal performance trade-offs. Reprint accepted for publication in Automatica, 2007.

[13] J. Schoukens, Y. Rolain, G. Simon, and R. Pintelon. Fully automated spectral analysis of periodic signals. *IEEE Transactions on Instrumentation and Measurement*, 52(4):1021–1024, 2003.

[14] M. Steinbuch. Repetitive control for systems with uncertain period-time. *Automatica*, 38(12):2103–2109, 2002.

[15] M. Steinbuch, S. Weiland, and T. Singh. Design of noise and period-time robust high order repetitive control, with application to optical storage. Reprint accepted for publication in Automatica, 2007.

[16] X. Zhang, T. Shinshi, L. Li, K.-B. Choi, and A. Shimokohbe. Precision control of radial magnetic bearing. In *Proceedings of the 10th International Conference on Precision Engineering*, pages 714–718, Yokohama, Japan, July 2001.

[17] X. Zhang, T. Shinshi, L. Li, and A. Shimokohbe. A combined repetitive control for precision rotation of magnetic bearing. *Precision Engineering*, 27:273–282, 2003.